

Imaging models for three-dimensional transmitted-light DIC microscopy

Chrysanthe Preza†, Donald L. Snyder†, José-Angel Conchello
Institute for Biomedical Computing
and †Department of Electrical Engineering
Washington University, St. Louis, Missouri

ABSTRACT

Nomarski Differential-Interference-Contrast (DIC) microscopy¹ is a widely used method for imaging transparent specimens that are not visible with ordinary light microscopy. DIC microscopy enhances contrast in the images of such specimens by converting differential phase changes to intensity variations via the method of light interference. These phase changes are introduced in light as it passes through regions of different refractive index within a specimen.

In this paper, the development of an imaging model that describes three-dimensional DIC imaging under partially-coherent illumination is presented. Our approach in deriving the model involves the derivation of a two-dimensional model and its extension to three dimensions, assuming weak optical interactions within the specimen. The coherent limit of our two-dimensional model coincides with existing DIC models. Model predictions generated with the coherent limit of the three-dimensional model are compared to real DIC images acquired from imaging phantom specimens. It is shown that the model predictions resemble the real images obtained with the condenser aperture closed better than the images obtained with the aperture open. This result confirms the need for the general model that we have derived.

Keywords: Nomarski DIC microscopy, imaging theory, 3D imaging, 3D microscopy

1 INTRODUCTION

During the past twenty years, the use of Nomarski Differential-Interference-Contrast (DIC) microscopy in the life sciences has grown to the extent that it is now probably the preferred optical system for obtaining phase information from unstained transparent and nonabsorptive biological specimens.² Such specimens, known as *phase objects*, cannot be seen when in-focus under an ordinary light microscope, but, because they retard or advance light that passes through them due to spatial variations in their refractive index and/or thickness, they can be examined with special microscopes that allow the visualization of phase variations. These phase variations can be converted to intensity variations for example by the use of interference methods. Nomarski DIC microscopy is one such interference method introduced to microscopy by G. Nomarski in 1953.³

In a DIC microscope, a two-dimensional (2D) image is formed from the interference of two mutually coherent waves that have a lateral differential displacement of a few tenths of a micrometer (called the *shear*) and are phase-shifted relative to each other.³ This is accomplished by illuminating a specimen with a plane-polarized beam that has been split into two orthogonally polarized, mutually coherent components by a Wollaston prism and afterwards recombined into a single beam by another prism and analyzer before being detected (see Figure 1). The amplitude, and thus the intensity of the resulting beam is a function of the phase difference between the two waves. Therefore, differences in the refractive index of neighboring points in the specimen produce differences in the intensity of the image, thus allowing the visualization of edges in transparent specimens. It can be shown, that the DIC image intensity is related to the gradient of the specimen's phase function (see Equation 6) which is a scaled version of the specimen's refractive index distribution. This property of DIC imaging makes the interpretation of DIC images difficult, especially because images obtained from the same object can vary greatly with different set-up parameters (see Figure 7), while images obtained from two different objects may look similar.^{4,5} Furthermore, the presence of a shadow-cast effect in the DIC images gives a false three-dimensional (3D) impression which may lead to inaccurate determination of the object's thickness.

DIC microscopes are used to study both two- and three-dimensional living specimens. An image of a 3D specimen

is obtained via the method of *optical sectioning* by collecting a set of 2D images (called the *optical sections*) while the specimen is moved through focus. Each 2D image contains information from the specimen plane that it is in-focus as well as contributions from specimen regions that are out of focus. This out-of-focus light degrades the images and thus must be removed either optically via confocal microscopes, or computationally.

Prior to the development of confocal microscopes, DIC microscopy was the preferred method for optical sectioning without the need for processing the images except for some contrast enhancement using the method of video-enhanced DIC.⁶ Video-enhanced DIC microscopy has been shown to possess good optical-sectioning capability and has often been used to visualize serial focal-plane images obtained from thick specimens.⁶ However, substantial out-of-focus light remains in DIC images.^{5,7}

As in other microscopy modalities, improvements in DIC images can be achieved by computational methods designed to undo degradations introduced by the optical system. A first step towards improving DIC images is the derivation of a reasonable imaging model that can predict these degradations.

In this paper, a general model for DIC image formation is presented, and results from testing the coherent limit of the model are shown. The paper is organized as follows. Section 2 summarizes related work. In Section 3, the model is derived for 2D imaging and then extended to three dimensions. Section 4 describes the data collection and the calculation of the model predictions. The last section is a comparison study between real DIC images and the model predictions.

2 RELATED WORK

Although a description of DIC optics can be found in previous publications,^{1,3,8} and in references therein, very little has been published concerning the mathematical theory of DIC image formation. All previous work on modeling DIC image formation has been based on the same two assumptions: 1) coherent illumination, and 2) weak optical interactions within the specimen, although, different approaches were used in model development. We briefly review related work below.

Galbraith⁹ predicted the DIC image of a point using computer simulations and compared it to the image of a pinhole for various imaging parameters. These images correspond to the squared magnitude of the DIC point-spread function (PSF), and we have used them as a reference for testing our software for the computation of the DIC PSF.

Holmes and Levy¹⁰ derived an expression for the intensity in a 2D DIC image. Simulated DIC images were generated using this expression and a computer generated phantom. Although these images were not compared to real DIC images, the authors reported that the images had a DIC appearance.

Cogswell and Sheppard⁷ derived a 2D transfer theory of image formation for DIC microscopy, and they compared the frequency transfer properties of a conventional DIC microscope to a confocal one for reflection optics. Their analysis showed that DIC images obtained with a nonconfocal microscope are degraded by out-of-focus light due to low spatial frequency components of defocused regions in the specimen. We have extended their frequency transfer theory to incorporate partially coherent illumination.

Dana⁵ developed a 3D linear model. Ignoring blurring due to the objective lens, Dana derived the ideal DIC image intensity (Equation 6), and then incorporated the diffraction effects due to the objective lens by blurring the ideal image intensity with the intensity PSF. However, this assumption is not valid for DIC imaging in which diffraction effects must be incorporated by blurring the image amplitude with the amplitude PSF. The deficiency of the model is evident in the differences observed in Dana's comparison of theoretical PSFs to images obtained from small beads.

3 MODEL FOR IMAGE FORMATION

Previous work on modeling DIC image formation^{5,7,10} is based on coherent illumination. However, in practice, ideal coherent illumination cannot be achieved in microscopes that use Köhler illumination because the condenser aperture

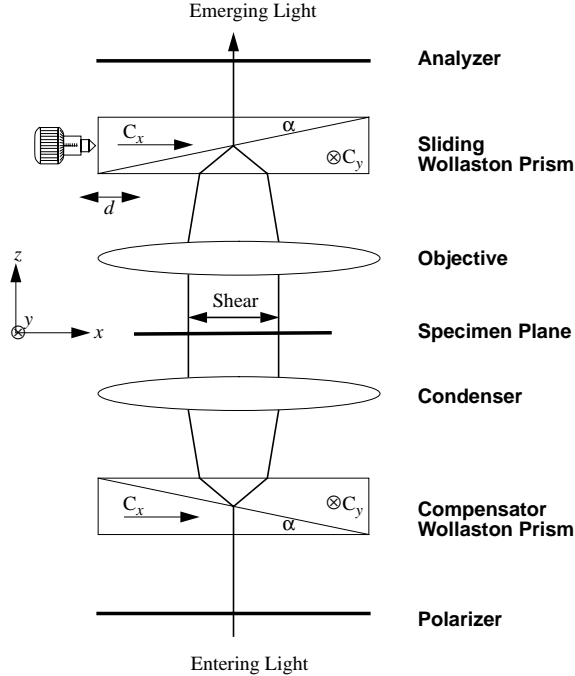


Figure 1: Schematic of the DIC microscope. Image formation with a DIC microscope is accomplished as follows. If the orientation of the polarizer is set so that its direction of light vibration is 45° relative to the x -axis, then the light emerging from the polarizer can be expressed by two orthogonal coherent components along the x - and y -axis. These two components are refracted differently by the compensator Wollaston prism yielding two waves which have a phase difference, and they are separated by the *shear*. The two waves then pass through different parts of the specimen, and thus when they are finally recombined by the sliding Wollaston prism, they have a different phase. Although, the sliding prism cancels the phase difference in the two waves introduced by the first prism (due to the way the two prisms are oriented), a translation, d , of the sliding prism along the x -axis introduces a uniform phase difference between the two components, called the *bias retardation*. Finally, the analyzer (which is crossed with the polarizer) passes light with only one polarization and, thereby, converts phase differences to amplitude differences.

cannot be stopped down to a single point. Even if this were possible it would not be desirable because it would degrade the resolution and reduce the illuminating light considerably. Thus, we have derived a 3D image formation model for DIC microscopy under partially coherent illumination, by first deriving a 2D model and then extending it to 3D assuming weak optical interactions within the specimen.

We have derived the 2D model by two different approaches, each of which led to the same result. First we extended the frequency theory of Cogswell and Sheppard⁷ from coherent to partially coherent illumination, based on the theory of image formation in partially coherent light for transmission optics described by Born and Wolf.¹¹ We arrived at the same model by propagating the complex amplitude of the illuminating wave-field under Köhler illumination through a thin specimen and the optical system. In the rest of this section, we first define the DIC PSF and then describe the model.

3.1 DIC point-spread function

In a DIC microscope, the image is formed from the difference between the amplitudes of two waves that are phase-shifted relative to each other, and are separated by a lateral *shear*, $2\Delta x$, (expressed in length units) introduced by the Wollaston prism (see Figure 1). Without loss of generality, we assume that the shear is along the x direction. The phase difference between the two waves is due to the fact that the waves travel through different regions of the specimen. Furthermore, a uniform phase difference between the two waves called the *bias retardation*, $2\Delta\theta$, (expressed in radians)

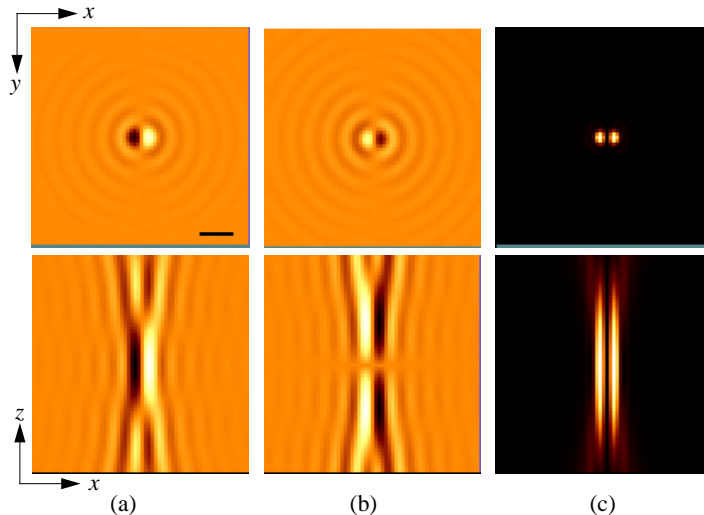


Figure 2: xy and xz images from a 3D calculated DIC PSF (of a 10×0.3 NA lens) with bias = 0 rads: (a) real part of the complex amplitude, (b) imaginary part of the complex amplitude, and (c) squared magnitude. For the xy images, $z = 1.7\mu\text{m}$ away from focus. The direction of shear is along the x -axis. The scale bar is approximately $3\mu\text{m}$.

can be introduced by translating the sliding prism along the shear direction. Assuming coherent illumination, when the phase difference due to the specimen is zero we can write the amplitude difference between the two waves as:

$$h(x, y) = (1 - R) e^{-j\Delta\theta} k(x - \Delta x, y) - R e^{j\Delta\theta} k(x + \Delta x, y), \quad (1)$$

where R is the *amplitude ratio* - the amplitude of one wave field divided by the sum of amplitudes of the two wave fields, and $k(x, y)$ is the amplitude PSF for transmission optics under coherent illumination.¹² The function $h(x, y)$ is the amplitude PSF for DIC optics under coherent illumination. The 3D PSF of a DIC system $h(x, y, z)$, and can be obtained from Equation 1 and the defocused PSF for transmission optics, $k(x, y, \Delta z)$, given in previous publications.^{13,14} Images of a calculated $h(x, y, z)$ are shown in Figure 2.

3.2 Derivation of the two-dimensional imaging model

The derivation given in this section is based on propagating the complex amplitude of the illuminating wave field under Köhler illumination through a thin specimen and the optical system. In Köhler illumination an extended light source emitting incoherent light is focused by a collector lens in the front-focal plane of the condenser lens¹¹ as shown in Figure 3. The condenser then illuminates the specimen which is specified by a complex amplitude transmission function $f(x, y)$, and is assumed to be planar with a small thickness and transparent with spatially varying refractive index. In the following analysis we consider paraxial light waves only, and assume that $f(x, y)$ is independent of the angle of illumination (i.e. the angle between the normal to the illuminating wave and the optical axis). We also assume that the light source is quasi-monochromatic with a mean wavelength λ . Let $[\xi, \eta]$, $[x_o, y_o]$, and $[x, y]$ denote points in the front-focal plane of the condenser lens, in the object plane, and in the image plane respectively.

Let the complex amplitude of the wave field in the front-focal plane of the condenser lens, $U_s(\xi, \eta)$, be a white random process with zero mean and covariance $E \{U_s(\xi, \eta)U_s^*(\xi', \eta')\} = \alpha(\xi, \eta) \delta(\xi - \xi', \eta - \eta')$, where $\alpha(\xi, \eta)$ is the intensity of the light source and equals zero at points that lie outside the circular aperture, D_c , of the condenser lens, $\delta(\xi, \eta)$ is a 2D impulse function, and $*$ denotes complex conjugate. Then the complex amplitude, $U_c(\xi, \eta)$, of the wave field in the back-focal plane of the condenser lens and right before the specimen can be obtained by the Fresnel superposition

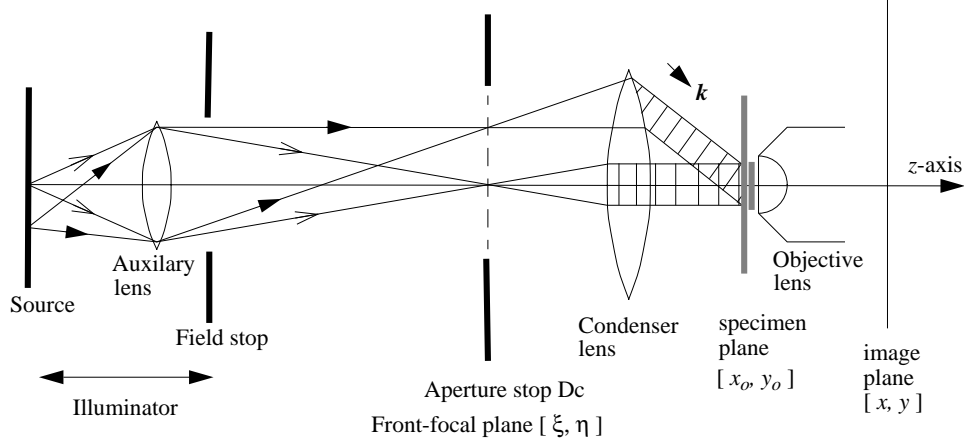


Figure 3: Köhler illumination. The specimen is illuminated by plane waves with normal vectors $\mathbf{k} = [k_x, k_y, k_z]$, $k_x = \frac{2\pi\xi}{\lambda f_c}$, $k_y = \frac{2\pi\eta}{\lambda f_c}$, $k_z = \sqrt{\left(\frac{2\pi}{\lambda}\right)^2 - k_x^2 - k_y^2}$, which make angles $\theta_x = \sin^{-1}\left(\frac{\xi}{f_c}\right)$ and $\theta_y = \sin^{-1}\left(\frac{\eta}{f_c}\right)$ with the yz - and xz -plane respectively (see p. 49 in Goodman¹⁵). The direction of illumination depends on the illuminating point $[\xi, \eta]$ in the front-focal plane of the condenser lens. The DIC components are not shown here for simplicity.

integral

$$U_c(x_o, y_o) = \int_{-\infty}^{+\infty} \int_{-\infty}^{+\infty} U_s(\xi, \eta) h_c(\xi, \eta; x_o, y_o) d\xi d\eta, \quad (2)$$

where $h_c(\xi, \eta; x_o, y_o) = \frac{1}{j\lambda f_c} e^{j2\pi(x_o\xi + y_o\eta)/\lambda f_c}$ specifies the complex amplitude of the illuminating plane waves (see Figure 3). Under the paraxial approximation the complex amplitude of the wave transmitted by the specimen is simply $U_o(x_o, y_o) = f(x_o, y_o) U_c(x_o, y_o)$. Assuming that the DIC microscope (excluding the condenser lens) is a linear shift-invariant system characterized by the PSF $h(x, y)$ (Equation 1), we can express the complex amplitude of the wave field in the image (detector) plane as

$$U_i(x, y) = \int_{-\infty}^{+\infty} \int_{-\infty}^{+\infty} U_o(x_o, y_o) h(x - x_o, y - y_o) dx_o dy_o. \quad (3)$$

The intensity in the image is then obtained from $i(x, y) = E\{U_i(x, y)U_i^*(x, y)\}$, which yields the expression

$$i(x, y) = \int_{-\infty}^{+\infty} \int_{-\infty}^{+\infty} \alpha(\xi, \eta) \left| \int_{-\infty}^{+\infty} \int_{-\infty}^{+\infty} f(x_o, y_o) h(x - x_o, y - y_o) h_c(\xi, \eta; x_o, y_o) dx_o dy_o \right|^2 d\xi d\eta. \quad (4)$$

Equation 4 is a general formulation of the intensity in the image plane of a DIC microscope and describes partially coherent imaging. Limiting cases of the model can be obtained by specifying the intensity, $\alpha(\xi, \eta)$, of the source. The coherent limit of the model, obtained by restricting $\alpha(\xi, \eta)$ to be zero except at a single point, predicts Holmes and Levy's¹⁰ intensity expression, and yields the same frequency transfer function reported by Cogswell and Sheppard⁷ (see Sections 3.3 and 3.4 below).

3.3 Coherent illumination

To describe coherent illumination we let $\alpha(\xi, \eta) = c_1 \delta(\xi, \eta)$ which corresponds to closing the condenser aperture down to a single point. In this case Equation 4 becomes

$$i(x, y) = c_1 \left| \int_{-\infty}^{+\infty} \int_{-\infty}^{+\infty} f(x_o, y_o) h(x - x_o, y - y_o) dx_o dy_o \right|^2. \quad (5)$$

It is easy to show that Equation 5 predicts the expression derived by Holmes and Levy.¹⁰ First we substitute Equation 1 (with $R = 0.5$) in Equation 5 and let $c(x, y) = \sqrt{c_1} e^{-j\Delta\theta} \int_{-\infty}^{+\infty} f(x_o, y_o) h(x - \Delta x - x_o, y - y_o) dx_o dy_o$. Then Equation 5 becomes $i(x, y) = |c(x, y) - e^{j2\Delta\theta} c(x + 2\Delta x, y)|^2$ which is the same as Equation 28 of Holmes and Levy¹⁰ with the specified shear and bias parameters.

It can be shown that for ideal imaging (i.e. ignoring the blurring effects of the PSF), Equation 5 becomes $i(x, y) = 4c_1 \sin^2(\frac{1}{2}[\phi(x - \Delta x, y) - \phi(x + \Delta x, y)] + \Delta\theta)$, where we have assumed that the specimen's transmission function is $f(x_o, y_o) = e^{-j\phi(x_o, y_o)}$ and, the PSF is $h(x, y) = e^{-j\Delta\theta} \delta(x - \Delta x, y) - e^{j\Delta\theta} \delta(x + \Delta x, y)$. Because the wavefront shear, $2\Delta x$, is very small (differential) relative to the size of the specimen, the difference in the phase can be written as a gradient yielding

$$i(x, y) = 4c_1 \sin^2 \left(\Delta x \frac{\partial \phi(x, y)}{\partial x} + \Delta\theta \right). \quad (6)$$

Thus, under coherent illumination and for ideal imaging the intensity in the DIC image is related to the gradient of the specimen's phase function along the direction of shear.

3.4 Frequency transfer theory

To compare our image formation model with the frequency transfer theory derived by Cogswell and Sheppard we first rewrite the detected intensity in terms of the mutual intensity of the wave field illuminating the specimen, $j_s(\mathbf{x}_o; \mathbf{x}'_o) = E \{U_c(\mathbf{x}_o) U_c^*(\mathbf{x}'_o)\}$,

$$i(\mathbf{x}) = \int_{-\infty}^{+\infty} \int_{-\infty}^{+\infty} f(\mathbf{x}_o) f^*(\mathbf{x}'_o) j_s(\mathbf{x}_o; \mathbf{x}'_o) h(\mathbf{x} - \mathbf{x}_o) h^*(\mathbf{x} - \mathbf{x}'_o) d\mathbf{x}_o d\mathbf{x}'_o, \quad (7)$$

where $\mathbf{x}_o = [x_o, y_o]$, $\mathbf{x}'_o = [x'_o, y'_o]$, and $\mathbf{x} = [x, y]$. We note that Equation 7 can be derived directly by propagating the mutual intensity, $j_s(\mathbf{x}_o; \mathbf{x}'_o)$, through the system in the same way that it was derived by others^{11,12} for transmitted optics. Equation 7 can then be rewritten (see Born and Wolf,¹¹ page 529) as

$$i(x, y) = \int_{-\infty}^{+\infty} \int_{-\infty}^{+\infty} \int_{-\infty}^{+\infty} \int_{-\infty}^{+\infty} T_{DIC}(f, g; f', g') F(f, g) F^*(f', g') e^{j2\pi[(f - f')x + (g - g')y]} df dg df' dg', \quad (8)$$

where $F(f, g)$ is the 2D Fourier transform of $f(x_o, y_o)$, and

$$T_{DIC}(\mathbf{f}'; \mathbf{f}'') = \int_{-\infty}^{+\infty} H(\mathbf{f} + \mathbf{f}') H^*(\mathbf{f} + \mathbf{f}'') J_s(\mathbf{f}) d\mathbf{f}, \quad (9)$$

is the transmission cross-coefficient of the system, where all bold letters denote vectors of spatial frequencies (i.e. $\mathbf{f}' = [f', g']$), and $H(\mathbf{f})$ and $J_s(\mathbf{f})$ are the Fourier transforms of $h(\mathbf{x})$ and $j_s(\mathbf{x})$ respectively. $T_{DIC}(\mathbf{f}; \mathbf{f}')$ expresses the combined effect of the illumination and the optics on the object, and characterizes the frequency transfer properties of

an optical system under partially coherent illumination as can be shown by the Fourier transform of the image intensity (Equation 8):

$$I(\mathbf{f}) = \int_{-\infty}^{+\infty} T_{DIC}(\mathbf{f}' + \mathbf{f}; \mathbf{f}') F(\mathbf{f}' + \mathbf{f}) F^*(\mathbf{f}') d\mathbf{f}'. \quad (10)$$

Another function that characterizes frequency transfer in an optical system under partially coherent illumination is the frequency response function of the system (see Born and Wolf,¹¹ p. 527) defined as

$$M_{DIC}(f, g; f', g') = H(f, g) H^*(-f', -g'), \quad (11)$$

which relates the Fourier transforms $J_o(\mathbf{f}; \mathbf{f}')$ and $J_i(\mathbf{f}; \mathbf{f}')$ of the mutual intensities at the object and image plane respectively as follows: $J_i(\mathbf{f}; \mathbf{f}') = M_{DIC}(\mathbf{f}; \mathbf{f}') J_o(\mathbf{f}; \mathbf{f}')$. The effective frequency response function for DIC, is obtained by inserting the Fourier transform of Equation 1 (which for $R = 0.5$ it is given by $H(f, g) = \frac{1}{j} \sin(2\pi f \Delta x + \Delta \theta) K(f, g)$) in Equation 11 yielding:

$$M_{DIC}(f', g'; f'', g'') = \sin(2\pi f' \Delta x + \Delta \phi) \sin(2\pi(-f'') \Delta x + \Delta \phi) M(f', g'; f'', g''), \quad (12)$$

where $K(f, g)$ and $M(\mathbf{f}'; \mathbf{f}'')$ are the transfer function and the frequency response function for transmitted optics respectively. We note that the expression reported by Cogswell and Sheppard (Equation 13 by Cogswell and Sheppard⁷) for the DIC transmission cross-coefficient is equal to $M_{DIC}(f', g'; -f'', -g'')$ and not to Equation 9. In order for the transmission cross-coefficient to take the same form as $M_{DIC}(f', g'; -f'', -g'')$ we must have $J_s(\mathbf{f}) = \delta(\mathbf{f})$ in Equation 9 which would correspond to the case of coherent illumination (see section 3.3). Thus, the result reported by Cogswell and Sheppard⁷) does not characterize a system under partially coherent illumination, but it is in fact the coherent limit of Equation 9.

3.5 Extension of the imaging model to three dimensions

Specimens used in DIC microscopy are considered to be *optically weak* which means that distortion of the wave field due to multiple refraction through the specimen can be regarded as a secondary effect. Thus, we have extended the 2D model (Equation 4) to 3D by assuming that an optically weak 3D object with thickness t along the z -axis, is a set of N planar specimens of thickness $\Delta z = t/N$, and that a wave field that interacts with one plane in the specimen does not interact with the other planes. This assumption is the first-order Born approximation (see Born and Wolf,¹¹ p. 453) which permits the use of linear superposition. A reasonable question here is what to superimpose: amplitudes or intensities? In order to answer this question, the issue of temporal coherence between two wave fields that interact with two different specimen planes that are a distance D_z apart must be examined. If temporal coherence exists then the two wave fields can interfere at the detector and thus the amplitudes of the different wave fields must be superimposed. On the other hand if the wave fields are temporally incoherent then the intensities of the wave fields can be superimposed.

To determine which case is the better approximation, one has to compare the coherence length of the illuminating source, l_c , to the smallest and largest possible distance D_z . The smallest D_z is the z -axis sampling distance, Δz , while the largest D_z is the thickness of the specimen, t . If $l_c \gg \bar{n}t$, where \bar{n} is the average refractive index of the specimen, then temporal coherence holds among all waves interacting with the specimen. On the other hand if $l_c \ll \bar{n}\Delta z$ then temporal incoherence holds between any two waves interacting with different specimen planes. For all other values of l_c temporal partial coherence holds. Because of the complexity of the partial coherence case, in practice assumptions are made in order to justify the use of temporal coherence or incoherence in the derivation of a model for a particular application. Instead of making any further assumptions, we derive two models: one based on superposition of amplitudes and the other of intensities, in order to determine which one is a better approximation. In what follows we present the two models.

When the image of a 3D object can be obtained by the superposition of the intensity images of the planes that make up the object, then the 3D image can be obtained by first introducing the specimen plane, z_o , in Equation 4:

$$i_{z_f}(x, y, z_f - z_o) = \int_{-\infty}^{+\infty} \int_{-\infty}^{+\infty} \alpha(\xi, \eta) \left| \int_{-\infty}^{+\infty} \int_{-\infty}^{+\infty} f(x_o, y_o, z_o) h(x - x_o, y - y_o, z_f - z_o) h_c(\xi, \eta; x_o, y_o) dx_o dy_o \right|^2 d\xi d\eta, \quad (13)$$

where z_f is the plane at which the microscope is focused, and then by integrating this intensity over all the specimen planes,

$$i(x, y, z) = \int_{-\infty}^{+\infty} i_{z_f}(x, y, z - z_o) dz_o, \quad (14)$$

where $h(x, y, z_f - z_o)$ is the 2D PSF defocused by a distance $\Delta z = z_f - z_o$. Alternatively, Equation 4 can be extended to 3D by integrating amplitudes over z_o , yielding a 3D intensity:

$$i(x, y, z) = \int_{-\infty}^{+\infty} \int_{-\infty}^{+\infty} \alpha(\xi, \eta) \left| \int_{-\infty}^{+\infty} \int_{-\infty}^{+\infty} \int_{-\infty}^{+\infty} f(x_o, y_o, z_o) h(x - x_o, y - y_o, z - z_o) h_c(\xi, \eta; x_o, y_o) dx_o dy_o dz_o \right|^2 d\xi d\eta. \quad (15)$$

To our knowledge, all existing 3D models for transmission optics are based on the first-order Born approximation,¹⁶⁻¹⁸ but it is unknown how realistic this approximation is in practice. We are planning on testing the two 3D models in order to determine how well they can predict real DIC data obtained from thick specimens.

4 METHODS

In order to test the model we have constructed two different phantom specimens for 3D DIC imaging. The phantom specimens were imaged with an Olympus IMT2 microscope using the IMT2-NIC attachment for DIC imaging, a 0.55 NA condenser lens, and a 10x 0.3 NA objective lens. A CCD camera was used to acquire the images. Imaging was performed with the condenser aperture either completely open or completely closed (for a closed aperture the effective condenser NA is 0.082) in order to compare them to model predictions for partially coherent and coherent illumination. Two different positions of the sliding prism were used in acquiring the images (one of the positions yielded a bias close to zero as judged visually by the dark background of the image).

4.1 Phantom specimens

The first phantom consists of a $4\mu\text{m}$ bead of refractive index $n_2 = 1.56$ embedded in an optical cement of refractive index $n_1 = 1.52$ (see Figure 4a). This phantom was chosen because it is easy to construct and its DIC images are simple to analyze. Images obtained with this phantom have pixel sizes $0.68\mu\text{m}$ in the x - y plane and the spacing along the z -axis is $6\mu\text{m}$.

The second phantom is a more challenging one, both in construction and imaging. This phantom is cross shaped - it consists of two perpendicular bars placed one on top of the other (see Figure 5a). The two bars have width, height and thickness of approximately $6\mu\text{m}$, and a refractive index higher than the refractive index of the medium that surrounds them. The phantom was constructed from resins of well known refractive indices¹⁹ with the use of a computer-driven laser beam (samples obtained with this process are called photo-defined waveguides). We have varied the refractive index difference between the bars and the surrounding medium, thereby constructing three phantoms of the same pattern but with different phase functions. This phantom was chosen because it has the ability to test the validity of intensity or amplitude superposition for weak specimens, an assumption that was used in extending the 2D model to 3D. The images obtained from this phantom have pixel sizes $0.68\mu\text{m}$ in the x - y plane and the spacing along the z -axis is $3\mu\text{m}$.

4.2 Simulations

Model predictions were obtained via simulations. For the simulations a theoretical PSF for the 10x 0.3 NA lens was first calculated using Equation 1 (see Figure 2). For the bead phantom a PSF with zero bias was used in the simulations. In the case of the crossed-bars phantoms PSFs with several different bias values (in the range $-0.03 < 2\Delta\theta < 0.03$ rads) were computed for the simulations. Computer generated phantoms that approximate the phantom specimens described above were used in the simulations. Simulated 3D DIC images were generated using a coherent illumination model (obtained from the *coherent limit* of Equation 15) which corresponds to having a point condenser aperture and assumes superposition of amplitudes. We chose this limiting case as a starting point because it is easier to compute than the

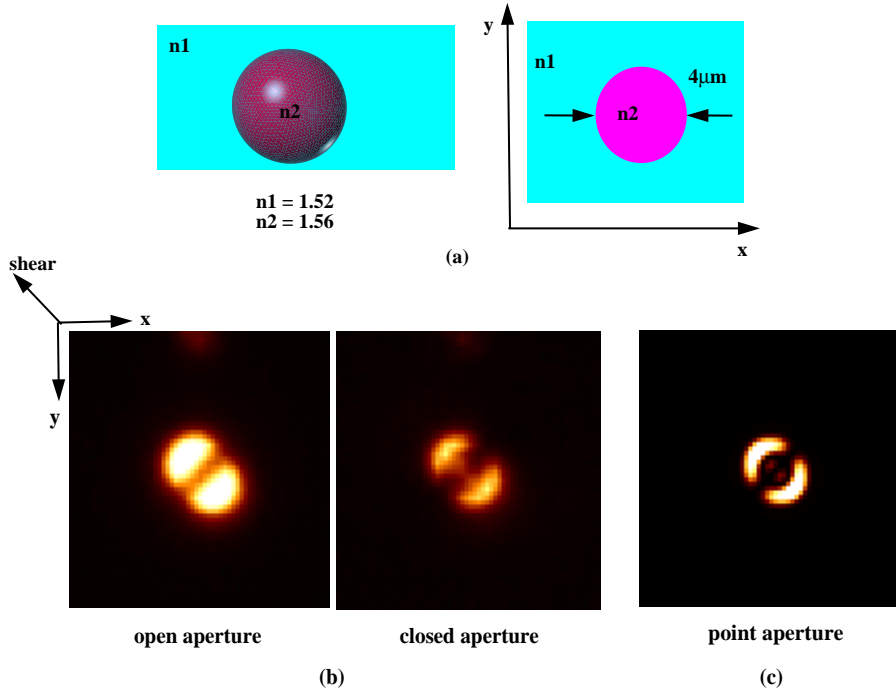


Figure 4: The bead phantom (a), and DIC images obtained with this phantom with the PSF bias equal to zero: (b) measured DIC images for two condenser apertures; (c) model prediction of the DIC image with a point condenser aperture.

general model and because it coincides with the 3D extension of existing models that have never been tested before with phantom specimens.

In the case of the crossed-bars phantom, simulated 3D DIC images were also generated using the *coherent limit* of Equation 14, in order to test the superposition of intensities assumption.

5 RESULTS

In this section we compare real DIC images to model predictions obtained from simulations for the bead and one of the crossed-bars phantom specimens (results obtained from the other two crossed-bars phantom specimens are similar and thus not included). For simplicity, 2D section images from the 3D images are shown in the figures. Figure 4b shows real DIC images acquired from the bead phantom specimen (the shown images correspond to the best focus). The image intensity is related to the derivative of the optical path along the direction of shear because of the DIC optics. The optical path changes at the edges of the bead but is constant in the center of the bead. The model prediction (shown in Figure 4c) is similar to the real DIC images, but because it was generated with a point condenser aperture it resembles the image acquired with a closed condenser aperture better than the image obtained with an open condenser aperture. A trend can be observed from the three images: the contrast increases as the condenser aperture decreases.

Figures 5 and 6 show images from the same crossed-bars phantom specimen for two different bias values. The 2D images shown were chosen so that both bars are in focus. Again, as in the case of the bead, the edges of the bars are highlighted in the DIC images. The model prediction (Figure 5c and Figure 6b) obtained by superimposing amplitudes is consistent with the measured images (shown in Figure 5b and Figure 6a). The contrast increases as the aperture decreases, and the model prediction compares better with the image obtained with a closed condenser aperture. In all the images, it can be seen that the edges of the bars are not equally bright. This feature is due to the non zero PSF bias and is more obvious in Figure 6 where the bias used is larger. The value of the bias determines how much brighter one

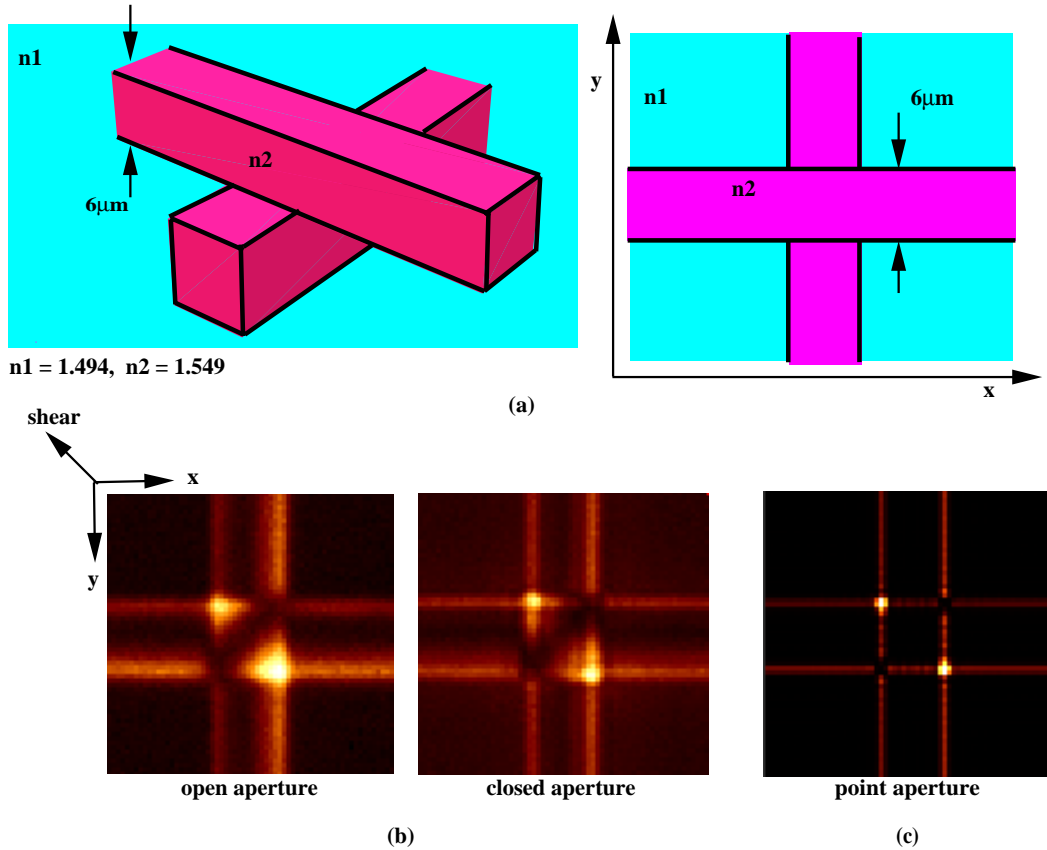


Figure 5: Phantom specimen with crossed bars (a), and DIC images obtained with this phantom: (b) measured DIC images for two condenser apertures; (c) model prediction of the DIC image obtained with a 3D model that assumes superposition of amplitudes and a point condenser aperture. The PSF bias is equal to -0.001 rads.

edge is, while the sign of the bias affects which edge of the bar is brighter (see Figure 7).

Figure 8 shows the model prediction obtained by superimposing intensities instead of amplitudes. In this case the model fails to capture the distinct features of the real DIC images. Thus for the testing conditions that we have used it appears that temporal coherence can be assumed and that superposition of amplitudes can be used in extending the 2D model to 3D.

6 SUMMARY AND CONCLUSIONS

The derivation of imaging models that describe 2D and 3D DIC imaging under partially-coherent illumination was presented. We have shown that the coherent limit of our 2D model coincides with existing DIC models. Model predictions obtained with the coherent limit of our 3D models were tested by imaging two different phantom specimens yielding two main results. First, comparisons between real DIC images and model predictions showed a number of similarities, but because the model predictions were generated for a point condenser aperture, they resembled real DIC images obtained with the condenser aperture closed better than with the aperture open. This result demonstrates the need for a general model that can predict images with the condenser aperture open. We are currently working on generating predictions from the general model.

Second, an issue raised in the extension of the 2D model to 3D about whether temporal coherence holds in DIC

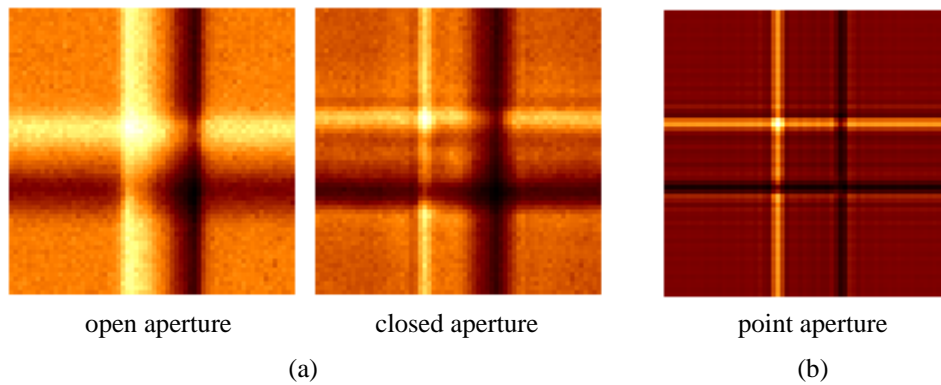


Figure 6: DIC images obtained with the phantom specimen shown in Figure 5a with PSF bias equal to 0.03 rads: (a) measured DIC images for two condenser apertures; (b) model prediction of the DIC image obtained with a 3D model that assumes superposition of amplitudes and a point condenser aperture.

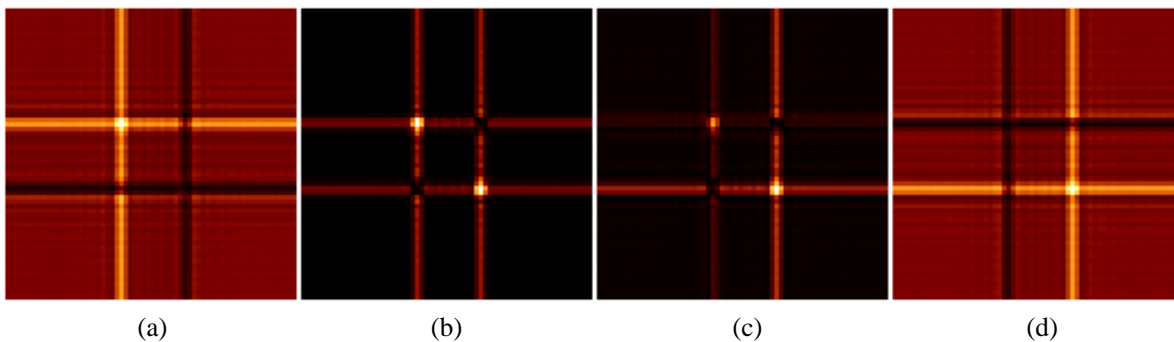


Figure 7: Model predictions of the DIC image of the phantom specimen shown in Figure 5a obtained with a 3D model that assumes superposition of amplitudes and a point condenser aperture, with PSF bias equal to: (a) 0.03, (b) 0.0, (c) -0.005, and (d) -0.03 rads.

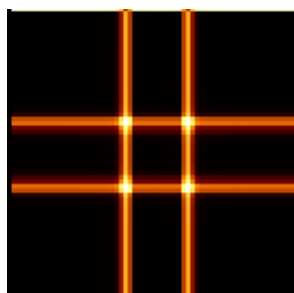


Figure 8: Model prediction of the DIC image of the phantom with the crossed bars obtained with a 3D model that assumes superposition of intensities and a point condenser aperture, with PSF bias equal to zero rads.

imaging was tested and resolved, at least for the one case tested so far. Model predictions generated with the 3D model based on superposition of amplitudes yielded predictions that resembled real DIC images much better than predictions generated with the model based on superposition of intensities, suggesting that temporal coherence is a better approximation.

7 ACKNOWLEDGEMENTS

This research was supported by the National Institutes of Health under research grant No. RR 01380. The authors wish to thank Robert Krchnavek and Richard Livingston for the construction of the crossed-bars phantom specimens, and James McNally for his help with acquiring the images and for insightful discussions.

8 REFERENCES

- [1] R. D. Allen, G. B. David, and G. Nomarski. “The Zeis-Nomarski Differential Interference Equipment for Transmitted-Light Microscopy”. *Zeitschrift für Wissenschaftliche Mikroskopie und Mikroskopische Technik*, 69(4):193–221, 1969.
- [2] H. Gundlach. “Phase Contrast and Differential Interference Contrast Instrumentation and Applications in Cell, Developmental, and Marine Biology”. *Optical Engineering*, 32(12):3223–3228, 1993.
- [3] M. Pluta. *Advanced Light Microscopy: Specialized Methods*, pages 146–197. Elsevier, Amsterdam, 1989.
- [4] W. Galbraith. “An Aid to Understanding Differential Interference Contrast Microscopy: Computer Simulation”. *Journal of Microscopy*, 108(2):147–176, 1976.
- [5] K. Dana. “Three Dimensional Reconstruction of the Tectorial Membrane: An Image Processing Method Using Nomarski Differential Interference Contrast Microscopy”. Master’s thesis, Massachusetts Institute of Technology, Massachusetts, 1992.
- [6] R. D. Allen, N. S. Allen, and J. L. Travis. “Video-Enhanced Contrast Differential Interference Contrast (AVEC-DIC) Microscopy: A New Method Capable of Analyzing Microtubule-Related Motility in the Reticulopodial Network of *Allogromia laticollaris*”. *Cell Motility*, 1:291–302, 1981.
- [7] C. J. Cogswell and C. J. R. Sheppard. “Confocal Differential Interference Contrast (DIC) Microscopy: Including a Theoretical Analysis of Conventional and Confocal DIC Imaging”. *Journal for Microscopy*, 165:81–101, 1992.
- [8] W. Lang. “Nomarski Differential Interference Contrast Microscopy”. *A Collection of Four Articles from Zeiss Information, Carl Zeiss, 7082 Oberkochen, West Germany*, 1968.
- [9] W. Galbraith. “The image of a Point of Light in Differential Interference Contrast Microscopy: Computer Simulation”. *Microscopica Acta*, 85(3):233–254, 1982.
- [10] T. J. Holmes and W. J. Levy. “Signal-Processing Characteristics of Differential-Interference-Contrast Microscopy”. *Applied Optics*, 26(18):3929–3939, 1987.
- [11] M. Born and E. Wolf. *Principles of Optics*, pages 526–532. Pergamon Press, Oxford, 1964.
- [12] J. W. Goodman. *Statistical Optics*, pages 286–324. John Wiley and Sons, New York, 1984.
- [13] H.H. Hopkins. “The Frequency Response of a Defocused Optical System”. *Proceedings of the Royal Society of London A*, 231:91–103, 1955.
- [14] F.S. Gibson and F. Lanni. “Diffraction by a Circular Aperture as a Model for Three-dimensional Optical Microscopy”. *J. Opt. Soc. Am. A*, 6(9):1357 – 1367, April 1989.
- [15] J. W. Goodman. *Introduction to Fourier Optics*. McGraw-Hill Book Company, New York, 1968.
- [16] N. Streibl. “Three-Dimensional Imaging by a Microscope”. *Journal of the Optical Society of America A*, 2(2):121–127, 1985.

- [17] I. Nemoto. “Three-Dimensional Imaging in Microscopy as an Extension of the Theory of two-Dimensional Imaging”. *Journal of the Optical Society of America A*, 5(11):1848–1851, 1988.
- [18] C. J. R. Sheppard and X. Q. Mao. “Three-Dimensional Imaging in a Microscope ”. *Journal of the Optical Society of America A*, 6(9):1260–1269, 1989.
- [19] K. Nakagawa. “Cross-linked Acrylic Polymers for Optical Waveguide Applications ”. Master’s thesis, Washington University, Sever Institute of Technology, St. Louis, Missouri, 1994.